frontiers | Frontiers in Earth Science

TYPE Methods
PUBLISHED 05 March 2025
DOI 10.3389/feart.2025.1510396

OPEN ACCESS

EDITED BY
Xiukun Wang,
China University of Petroleum, Beijing, China

REVIEWED BY
Zhongwei Wu,
Yangtze University, China
Jun Yang,
Changzhou University, China

*CORRESPONDENCE
Xiaomei Zheng,
1196312948@qq.com
Chengqian Tan,
1098364810@qq.com

RECEIVED 12 October 2024
ACCEPTED 03 February 2025
PUBLISHED 05 March 2025

CITATION
Zheng X, Qiu X, Wang Z, He X, Li S, Tan C, Pan J and Luo X (2025) Study on quantitative characterization of microscopic pore throat in tight oil reservoir.
Front. Earth Sci. 13:1510396.
doi: 10.3389/feart.2025.1510396

Study on quantitative characterization of microscopic pore throat in tight oil reservoir

Xiaomei Zheng[1]*, Xiangliang Qiu[2], Zhengquan Wang[3], Xin He[3], Sunyi Li[3], Chengqian Tan[4]*, Jingyu Pan[5] and Xiang Luo[4]

[1]China National Petroleum Corporation Oriental Geophysical Exploration Co. Ltd. Urumqi Branch of the Research, Urumqi, China, [2]Chuanqing Drilling and Exploration Engineering Co., Ltd. Changqing Downhole Technology Operation Company, Xi'an, China, [3]PetroChina Changqing Oilfield Company Plant No.7, Xi'an, China, [4]School of Earth Science and Engineering, Xi'an Shiyou University, Xi'an, China, [5]China PetroChemical News, Beijing, China

Tight oil reservoirs exhibit poor physical properties, significant heterogeneity, and intricate pore structures. The investigation of the microscopic pore-throat structure plays a pivotal role in assessing the efficacy of these reservoirs. Using the Chang 8 reservoir in the Yanchi area of the Ordos Basin as a case study, conventional experimental methods were used to analyze and test its pore structure and evaluate the micro pore structure characteristics of the reservoir in this area, but due to the large amount of experimental data obtained by the conventional experimental methods and the difficulty of analyzing them, so we proposed a method of logging and evaluating the quality of the microscopic pore throats. By carrying out the research on the quantitative characterization relationship between the microscopic pore structure parameters and microscopic pore-throat quality of the tight reservoir, the pore-throat quality logging evaluation index PTI was obtained, and the quantitative evaluation standard of microscopic pore-throat quality of the tight sandstone reservoir was established. The findings indicate the following: (1) The predominant pore types within the Chang 8 reservoir in the study region consist mainly of intergranular pores and feldspar dissolved pores, showing an average surface porosity of 3.3%. The reservoir predominantly comprises nano-scale pore throats, contributing to its dense nature. Fluid seepage capacity is primarily governed by relatively larger pores. The main throat radius falls within the range of 101–601 nm, with an average pore throat ratio mainly ranging between 102 and 199. The average movable fluid saturation is measured at 26.51%. (2) After thorough analysis, it has been discerned that four key parameters—porosity (φ), median radius (R_{pt50}), displacement pressure (P_d), and maximum pore throat radius (R_{max})—exert significant influence on pore throat quality. Consequently, a logging evaluation index, *PTI* (Pore Throat Index), has been devised to gauge pore throat quality, accompanied by the establishment of a quantitative evaluation standard for the microscopic pore throat quality of tight sandstone reservoirs. (3) The reservoirs within the research area are categorized into four groups: I, II, III, and IV. A higher *PTI* value indicates superior pore throat quality, leading to an overall enhanced reservoir evaluation. This quantitative evaluation method is of guiding significance for the quantitative characterization of micropore throats in tight oil reservoirs and the efficient development of the oil field in this area, and it is also of some reference significance for the

quantitative characterization of micropore throats in similar tight sandstone reservoirs.

KEYWORDS

tight oil reservoir, microscopic pore-throat structure, quality evaluation of pore throat, Chang 8 reservoir, reservoir evaluation

1 Introduction

With the advancement of oil and gas exploration and the evolution of oil and gas resources, tight oil is assuming an increasingly crucial role in resource exploration and stands out as a significant unconventional source of oil and gas (Jia et al., 2012; Zou et al., 2012). The microscopic pore-throat structure within the reservoir has a direct impact on hydrocarbon enrichment, subsequent development challenges, and overall development effectiveness (LV et al., 2020). Hence, it is imperative to conduct research on the quantitative characterization methods for the microscopic pore-throat structures within tight oil reservoirs.

Researchers both domestically and internationally have dedicated significant efforts to the exploration of reservoir microscopic pore-throat structures. The examination of these structures is primarily achieved through various advanced techniques such as casting thin sections, scanning electron microscopy, high-pressure mercury intrusion, and nuclear magnetic resonance (Deng et al., 2018; Chai et al., 2023; Wu et al., 2021; Hong et al., 2020). These technical experimental methods allow for a meticulous characterization of the microscopic spatial and pore structure features within dense reservoirs (Li et al., 2020; Liu et al., 2018) characterized the reservoir space microscopic pore-throat features of tight reservoirs by fine inscription based on a combination of algorithms and experimental methods, and clarified the influence of pore-throat features on porosity and permeability (Chen et al., 2019), for instance, integrated mercury intrusion porosimetry with nuclear magnetic resonance to reconstruct the overall pore throat size distribution, employing equivalent triangular cross-section pores. Their work focused on evaluating tight sandstone reservoirs, revealing the influence of microstructure on reservoir quality and fluid distribution (Li et al., 2022) utilized a combination of mercury injection capillary pressure and low-field nuclear magnetic resonance to assess the pore size distribution of Chang 7 tight sandstone reservoir, exposing distinct profiles of pore structure within tight sandstone reservoirs (Ouyang et al., 2023) investigated throat radius, pore throat, and pore area through an amalgamation of improved nuclear magnetic resonance and rate-controlled porosity, elucidating the distribution mechanism of movable fluid in different spaces. Their work clarified the influence of pore throat characteristics on porosity and permeability. Building on casting thin section analysis, scanning electron microscopy, high-pressure mercury injection, and nuclear magnetic resonance tests (Huang et al., 2020), established a classification standard for the pore structure of target reservoirs. Proposed an evaluation method for assessing the pore connectivity of tight reservoirs, utilizing high-pressure mercury injection and nuclear magnetic resonance, and validated its rationality and feasibility through spontaneous imbibition experiments. Concurrently (Lai et al., 2014), introduced the mathematical evaluation method of cluster analysis into the microscopic pore structure analysis of tight reservoirs.

In summary, previous research on the microscopic pore structure of reservoirs commonly employs scanning electron microscopy to observe the characteristics of micro-nano pores. Techniques such as high-pressure mercury injection, constant-rate mercury injection, and nuclear magnetic resonance are utilized to investigate the distribution characteristics of microscopic pore throats. Additionally, mathematical fractal theory is employed to characterize the heterogeneity of pore structure. Nevertheless, the strong heterogeneity of the microscopic pore structure in tight sandstone reservoirs, encompassing diverse pore types and significant changes in pore structure, poses challenges. Traditional methods often analyze the influence on pore throat quality from the perspective of a single factor, making it difficult to accurately and quantitatively characterize the quality of pore throats in tight oil reservoirs. This challenge has emerged as a technical bottleneck restricting the development of tight oil (Zou et al., 2019; Zhao et al., 2020; Morozov et al., 2021; Alessa et al., 2021).

Consequently, this study focuses on the Chang 8 tight oil reservoir in the Yanchi area. Leveraging test data from casting thin sections and scanning electron microscopy, it delves into the petrological composition and structural characteristics of tight oil reservoirs. High-pressure mercury injection and nuclear magnetic resonance are employed to analyze the pore throat structure characteristics of tight reservoirs. The paper utilizes quantitative evaluation parameters of microscopic pore throat quality to explore pore structure types, providing a comprehensive understanding of the influence of microscopic pore structure parameters on the microscopic pore throat quality of reservoirs. The study proposes a new method for quantitatively characterizing the microscopic pore structure of tight reservoirs, contributing to the enrichment of current characterization parameters for microscopic pore structure. This research offers a reliable microscopic geological foundation for identifying the “dessert area” of tight sandstone reservoirs and facilitating their subsequent efficient development and enhanced oil and gas recovery. The study of microscopic pore throat quantitative characterization technology of reservoir can understand the law of oil and gas generation, migration and accumulation, and provide technical support for the development and utilization of unconventional oil and gas resources.

2 Geological background

The Yanchi area in the study area is located in the northwest of the Ordos Basin, belonging to the central and western part

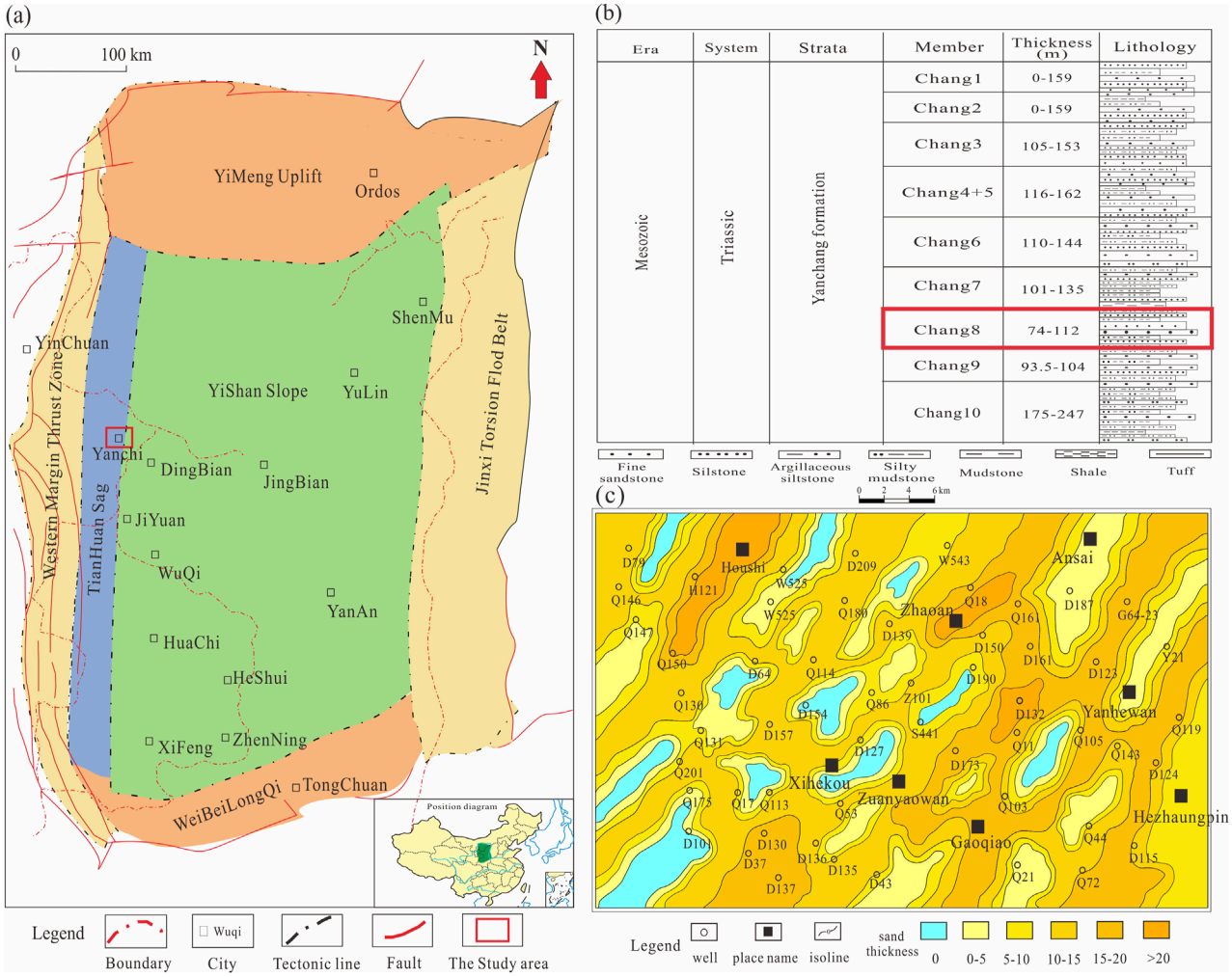

FIGURE 1
Regional location map of the study areas **(a)**. Stratigraphic delineation map **(b)**. Sand body thickness map **(c)**.

of the Yishan slope. It spans the two major tectonic units of the thrust belt on the western margin of the basin and the Tianhuan depression (Figure 1A) (Wang et al., 2022; Yang et al., 2023), as shown in Figure 1.

In the study area, our focus is on the Chang 8 formation, which exhibits a total thickness ranging from approximately 74–112 m. By considering vertical lithological variations and depositional rotations, the Chang 8 oil layer group is further stratified into the Chang 8_1 and Chang 8_2 subsections (Figure 1B). The Chang 8 sand body, characterized by substantial thickness and extensive distribution, predominantly consists of a composite underwater distributary channel sand body comprising contiguous sheets and bands (Figure 1C). The structural stability of the Chang 8 formation in the study area is notable, with local formations experiencing low-amplitude uplift due to tectonic stress. This uplift generates micro-fractures that enhance reservoir connectivity (Zuo et al., 2019), positively impacting reservoir permeability. In a stable tectonic environment, the provenance primarily originates from the northeast Yinshan ancient land and the northwest Alashan ancient land, indicative of delta front deposition. The underwater distributary channel sand body dominates, featuring fine sediment grain size and a distribution along the northeast-southwest belt. The sand body exhibits considerable thickness with excellent horizontal and vertical continuity (Nie et al., 2020; Fan et al., 2023), establishing favorable reservoir conditions for the Chang 8 oil layer group, our target layer. The physical properties of the Chang 8 reservoir in the study area are characterized by poor conditions, primarily influenced by the combined effects of sedimentation, structure, and diagenesis. With an average porosity of 7% and an average permeability of $0.16 \times 10^{-3}\mu m^2$, the reservoir falls into the category of ultra-low porosity and ultra-low permeability. Over its long geological history, the Chang 8 reservoir has undergone complex diagenesis, presenting tight lithology, poor physical properties, diverse pore types, complex structure, and strong heterogeneity (Kong et al., 2023; Wang et al., 2020). These factors significantly impact the exploration and development of tight oil in the study area.

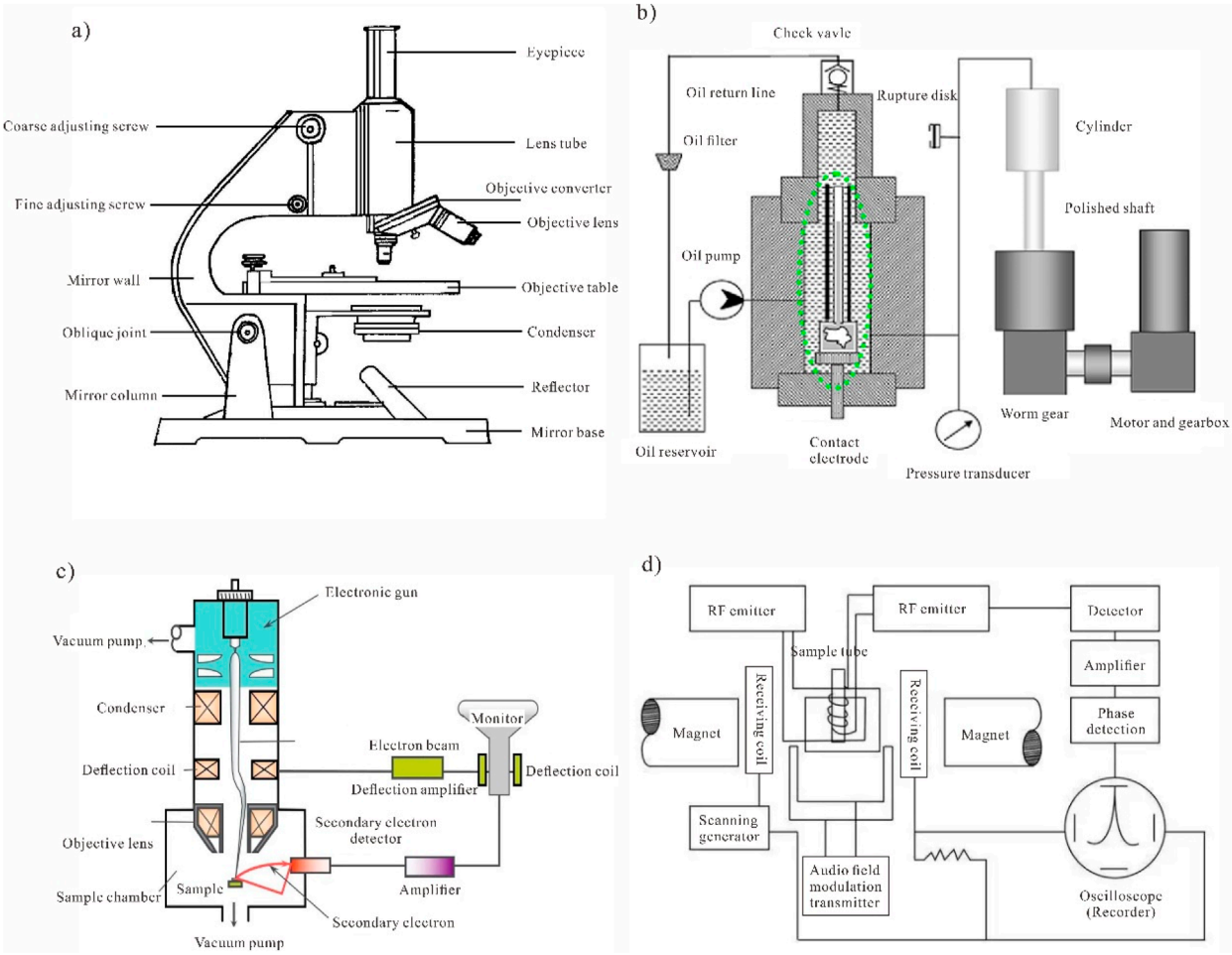

FIGURE 2
Schematic diagram of the working principle of the experimental method of microscopic pore structure (**(a)**. Schematic diagram of a polarized light microscope **(b)**. Schematic diagram of the working principle of a sweeping electron microscope **(c)**. Schematic diagram of the working principle of mercury pressure meter **(d)**. Schematic diagram of the working principle of nuclear magnetic resonance instrument).

3 Experimental methods and produces

3.1 Experimental method of microscopic pore structure

In this investigation, 20 samples were meticulously chosen for experimental analysis (Supplementary Annex 1). Given the low permeability of the sandstone reservoirs under study, conventional methods for characterizing pore-throat structures were employed. These methods include casting thin section identification, scanning electron microscopy, high-pressure mercury injection, and nuclear magnetic resonance. These techniques enable both qualitative and quantitative analyses of the pore-throat structure in low permeability reservoirs (Klaver et al., 2015; Wang B. et al., 2021; Zou et al., 2019; Yin et al., 2019; Singh et al., 2022).

3.1.1 Casting thin section identification

The analysis of the cast thin sections adhered to the guidelines outlined in "Classification of Rock Pore Types in Oil and Gas Reservoirs" (SY/T 6173-1995), utilizing a polarizing microscope model DM4500P (Figure 2A). During observation, an accelerating voltage of 20 kV, a resolution of 1μm, and a spot size of 4 μm were employed. The experimental temperature was maintained at 20°C. This meticulous process allows for a comprehensive examination of the microscopic features within rock formations, providing valuable insights into pore structures and connectivity.

Experimental principle and method: In the process of casting thin sections, dyed resin or liquid glue, often in shades of blue or red, is injected into rock pores within a vacuum environment. The resin or liquid glue is then subjected to specific temperature and pressure conditions, after which it is finely ground into thin sections. Subsequently, these thin sections are examined under a polarized light microscope to observe the characteristics of pores, throats, their connectivity, and the spatial arrangement of pores.

3.1.2 Scanning electron microscopy

Scanning electron microscopy represents a cutting-edge electron optical instrument employed for surface structure observation of objects (Figure 2B). The scanning electron

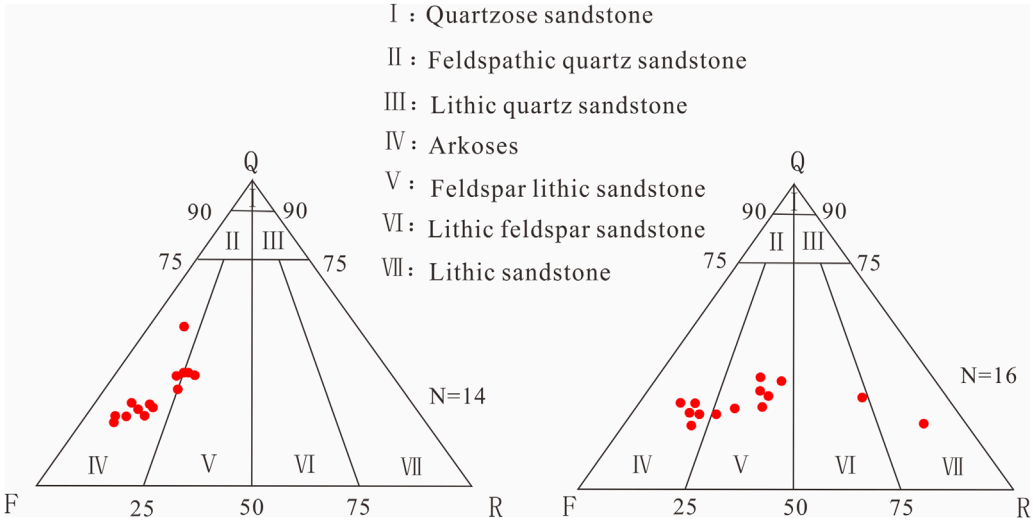

FIGURE 3
Reservoir sandstone classification of Chang 8_1 and Chang 8_2 in the study area **(a)**. Rocks Classification map of Chang 8_1 **(b)**. Rocks Classification map of Chang 8_2.

microscope utilized for the analysis experiments in this study is the JSM-6390A scanning electron microscope, conducted within a vacuum environment. The accuracy of the scanning electron microscope surpasses that of a typical optical microscope, boasting a resolution typically ranging from a few nanometers to several dozen nanometers. This advanced technology enables a meticulous exploration of surface features, providing invaluable insights into the structural intricacies of the examined samples (Zhong et al., 2023; Kong et al., 2023).

Principle of the experiment: The fundamental principle involves directing a finely focused electron beam onto the sample's surface. As a consequence of the interaction between the high-energy electron beam and the sample material, various signals such as secondary electrons, backscattered electrons, absorbed electrons, X-rays, cathodoluminescence, Russo-cycles, and transmission electrons undergo changes in response to the surface morphology of the measured sample.

3.1.3 High pressure mercury intrusion

High-pressure mercury injection (Figure 2C), also referred to as constant pressure mercury injection or conventional mercury injection, stands out as one of the most widely employed methods in rock reservoir evaluation. This method involves injecting mercury into the non-wetting phase fluid within the rock, measuring the quantity of mercury injected into the rock under a specific constant pressure. The obtained relationship curve between mercury injection pressure and the injected mercury quantity or saturation provides crucial insights. The calculation involves determining the pore volume controlled by the pore throat at different mercury injection pressures, allowing for the derivation of the rock's pore size distribution (Wang D. et al., 2021; Lu Z. D. et al., 2022; Wang et al., 2021c). The experiment follows the standards outlined in the "Rock Capillary Pressure Curve Determination" SY/T5346-2005. The AutoPore IV 9505 mercury pressure meter serves as the experimental instrument, maintaining a controlled environment at a temperature of 22°C, humidity at 60%, and precision within the range of 10 nm to ten microns. This meticulous approach ensures accurate and reliable results in characterizing the pore structure of the rock under high-pressure mercury intrusion (Liu et al., 2023; Zhao et al., 2021).

Experimental method and procedure: When the mercury inlet pressure increases from P_1 to P_2, the corresponding pore size decreases from r_1 to r_2, and the amount of mercury inlet at this stage is the corresponding pore volume between the two pore sizes. When the mercury inlet pressure is continuously increased, the mercury inlet volume of different pore sizes can be measured.

3.1.4 Nuclear magnetic resonance

The fundamental principle of nuclear magnetic resonance technology involves harnessing the inherent magnetism of hydrogen nuclei and their interaction with an external magnetic field (Figure 2D). By measuring the amplitude and relaxation rate of the nuclear magnetic resonance signal of hydrogen nuclei within the rock's pore fluids, this method provides insights into the rock's pore structure and related fluid properties (Zhao et al., 2014; Zhou et al., 2022). During the measurement of the NMR T_2 spectrum of fluid-saturated rock samples, the size and distribution characteristics of the NMR T_2 relaxation time of the fluid enable analysis of the fluid's occurrence state within the rock pores (Bai et al., 2016). The nuclear magnetic resonance rock sample analyzer, denoted as Micro-MR02, serves as the experimental instrument for these investigations. The experiments are conducted in an environment maintained at 25°C and 97.6Kpa, ensuring precise measurements within the range of 8 nm to eighty microns.

Experimental methods and steps: ①Drill a standard core with a diameter of 25.4 mm from a full-diameter core; ②Wash the standard core of residual oil and dry it; ③Measure the permeability of the core using nitrogen; ④After the core is vacuumed, saturate the core with simulated formation water at a pressure of 24 MPa; ⑤Remove the movable water from the core in centrifugation experiments

10.3389/feart.2025.1510396

TABLE 1 Statistical table of detrital components of Chang 8 reservoir in the study area (unit: %).

Layer	Sample	Quartz	Feldspar	Debris				Miscellaneous		Fillings
				Igneous rock debris	Metamorphic rock debris	Sedimentary rock debris	Total	Mica	Chlorite	
$Chang8_1$	16	26.44	50.09	2.06	5.56	0.00	7.63	3.06	0.88	11.84
$Chang8_2$	14	23.00	40.46	4.07	7.11	0.32	11.5	2.89	6.14	15.43

and sample the T_2 spectra of the centrifuged core; ⑥Compare the T_2 spectral distribution before and after centrifugation to calculate the movable water saturation and porosity; ⑦Use NMR to sample the core in saturated simulated formation water using NMR. T_2 spectrum distribution before and after centrifugation, the movable water saturation and porosity were calculated; ⑧NMR T_2 test was performed on the core saturated with simulated formation water using an NMR instrument.

3.2 Methods for microscopic pore-throat quality logging evaluating

To swiftly comprehend the microscopic pore structure characteristics inherent in tight reservoirs, a comprehensive investigation into the quantitative relationship between microscopic pore structure parameters and the quality of microscopic pore throats in tight reservoirs has been undertaken. This endeavor resulted in the derivation of the Pore Throat Quality Logging Evaluation Index (PTI) and the establishment of a quantitative standard for assessing the microscopic pore-throat quality in tight sandstone reservoirs. The pore throat quality logging evaluation index (PTI) is a comprehensive index utilized to assess the quality of reservoir pore throat. It integrates various structural parameters of pore throats and quantitatively evaluates the microscopic characteristics of these reservoirs through mathematical modeling and statistical analysis techniques.The capillary pressure curve of the tight oil reservoir is established using mercury intrusion and nuclear magnetic resonance data. Subsequently, multiple mathematical models are employed to calculate the microscopic pore-throat characteristic parameters of the shale oil reservoir, and the pore-throat quality evaluation index is constructed based on these parameters. Finally, the pore-throat quality of the tight oil reservoir was classified into different categories according to the evaluation index, and the high-quality reservoir was effectively identified. The initial step involves standardizing the samples, ensuring data values are confined within the range of 0 and 1. This normalization process eradicates differences in dimensions and orders of magnitude among various variables. Subsequently, the factor analysis method is employed to reduce data dimensions, extracting the initial eigenvalues from the correlation coefficient matrix. Finally, a comprehensive analysis of diverse influencing factors culminates in the identification of key factors that significantly impact the microscopic pore-throat quality within tight reservoirs. This approach not only streamlines the evaluation process but also enhances the understanding of the critical parameters governing the microscopic characteristics of tight sandstone reservoirs.

1) Data Standardization. Assuming a total of m feature parameters and n wells. x_{ij} denotes the jth characteristic parameter of the ith well, and x_{ij} is converted into the standard feature parameter $\overline{X}_{ij}$, achieved through the following Formula 1:

$$\overline{X}_{ij} = \frac{x_{ij} - \overline{x}_j}{S_j}, (i = 1, 2, \cdots, n; j = 1, 2, \cdots, m) \quad (1)$$

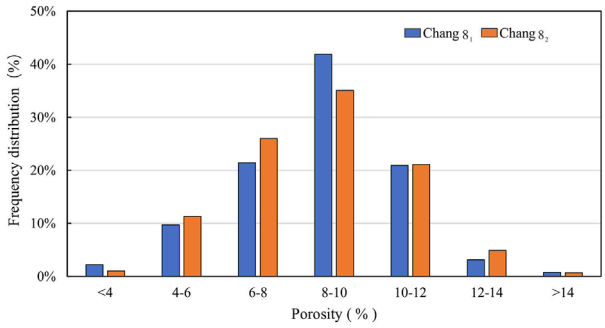

FIGURE 4
Histogram of Chang 8 porosity distribution in the study area.

Among them (Formula 1):

$$x_j = \frac{1}{n}\sum_{i=1}^{n} x_{ij} \tag{2}$$

$$S_j = \frac{1}{n-1}\sum_{i=1}^{n}\left(x_{ij} - \overline{x}_j\right)^2 \tag{3}$$

Herein:

$\overline{X}_{ij}$ represents the *jth* characteristic parameter of the *ith* well; $\overline{x}_j$ is the average value of the *jth* characteristic parameter (Formula 2); S_j is the standard deviation of the *jth* characteristic parameter (Formula 3).

Correspondingly, $\overline{x}_i = \frac{x_i - \overline{x}_i}{S_i}$ is the characteristic parameter variable of each well after standardization (Formula 4).

$$\overline{x}_i = \frac{x_i - \overline{x}_i}{S_i} \tag{4}$$

Herein:

$\overline{x}_i$ is the average value of the *i* well, S_i is the standard deviation of the *ith* well.

2) Establishing the correlation coefficient matrix R between the characteristic parameters (Formula 5), namely:

$$R = \left(r_{ij}\right)_{m\cdot n} \tag{5}$$

$$r_{ij} = \frac{\sum_{k=1}^{n} \overline{X}_{ki} \cdot \overline{X}_{kj}}{n-1} \tag{6}$$

Herein:

u_j r_{ji} is the index of the relationship between *i* and *j*, and $r_{ij} = r_{ji}$; $\overline{X}_{ki}$ is the standard value of the *ith* characteristic parameter of the *kth* well (Formula 6).

3) Finding the correlation coefficient matrix *R*, with eigenvalues λ_j, that is $\lambda_1 \geq \lambda_2 \geq \cdots \geq \lambda_m \geq 0$,the eigenvector is c_j, that is Formula 7:

$$c_j = \left(c_{1j}, c_{2j}, \cdots, c_{nj}\right)^T \tag{7}$$

The feature vector is composed of *m* new parameters, namely *m* main influencing factors, $(F_1, F_2, \cdots, F_m)$,which can be set as follows (Formula 8):

$$\begin{cases} F_1 = c_{11}\overline{X}_1 + c_{21}\overline{X}_2 + \cdots + c_{n1}\overline{X}_n \\ F_2 = c_{12}\overline{X}_1 + c_{22}\overline{X}_2 + \cdots + c_{n2}\overline{X}_n \\ \cdots\cdots \\ F_m = c_{1m}\overline{X}_1 + c_{2m}\overline{X}_2 + \cdots + c_{nm}\overline{X}_n \end{cases} \tag{8}$$

4) The comprehensive scores of the main influencing factors were calculated. Firstly, the information contribution rate and cumulative contribution rate of eigenvalue λ_j are calculated:

$$\omega_j = \frac{\lambda_j}{\sum_{k=1}^{n}\lambda_k} \tag{9}$$

$$\alpha_p = \frac{\sum_{k=1}^{p}\lambda_k}{\sum_{n=1}^{n}\lambda_k} \tag{10}$$

λ_k is the eigenvalue of the *kth* well, ω_j is the information contribution rate of the *jth* main influencing factor, α_p is the cumulative contribution rate of *p* main influencing factors (Formulas 9, 10).

Finally, when α_p is close to 1, the first *p* influencing factors F_j are taken as the main influencing factors to replace *m* new parameters, so as to comprehensively analyze the *p* influencing factors. Calculate the comprehensive score *F* (Formula 11):

$$F = \sum_{j=1}^{n} \omega_j F_j \tag{11}$$

F is regarded as the logging evaluation index *PTI* of pore throat quality, F_1 is the main controlling factor affecting the quality of pore throat, F_2 is the secondary factor, and so on. The inference formula of the logging evaluation index *PTI* of pore throat quality is obtained as follows (Formula 12):

$$PTI = \omega_1 F_1 + \omega_2 F_2 + \omega_3 F_3 + \cdots + \omega_j F_n \tag{12}$$

4 Results and discussion

4.1 Characterization of reservoir pore throat structure

Based on the comprehensive analysis of core drilling, core observations, and rock samples within the study area, notable distinctions were identified in the rock types between the Chang 8_1 and Chang 8_2 oil layers. The predominant rock type in the Chang 8_1 oil layer group is feldspar sandstone, while the Chang 8_2 oil layer group exhibits dominance in feldspar sandstone and feldspar lithic sandstone (refer to Figure 3). The rock particles display a fine size, mostly characterized as fine sand, with observable

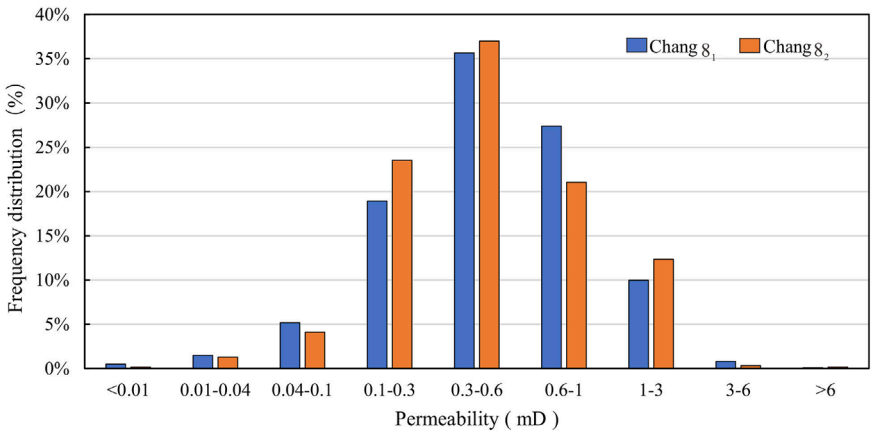

FIGURE 5
Histogram of Chang 8 permeability distribution in the study area.

coarse and uneven particles indicating conditions of relatively deep-water bodies during the sedimentary period. In terms of detrital components, the Chang 8_1 oil layer group comprises 88.1% of the total rock, the Chang 8_2 oil layer group comprises 83.99%, and the entire Chang 8 oil layer group comprises 86.04%. The average quartz content is 24.72%, feldspar constitutes an average of 45.27%, and debris contributes an average of 19.13%. Metamorphic rock debris holds the highest content, followed by igneous rock debris, with almost negligible sedimentary rock debris (Table 1). The content and proportion of terrigenous debris exhibit significant variability, often accompanied by a substantial matrix formation, playing a pivotal role in determining the physical properties of the reservoir.

The study area exhibits strong reservoir heterogeneity and notably poor physical properties (Clarkson et al., 2013; Lai et al., 2014; Zhao et al., 2020), illustrated in Figures 4, 5. Core analysis data from 217 samples in the study area reveal that the porosity of the Chang 8 reservoir predominantly falls within the range of 4%–12%, with a median porosity of 7%. Permeability is primarily distributed between $0.01 \times 10^{-3}\mu m^2$ and $0.3 \times 10^{-3}\mu m^2$, with a median permeability of $0.16 \times 10^{-3}\mu m^2$. Applying the classification criteria for clastic rock reservoirs, the study area is classified as having low porosity and ultra-low permeability reservoirs (Lan et al., 2021; Liu et al., 2022; Jing et al., 2023; Mahdaviara et al., 2021).

Observations of casting thin sections from the Chang 8 reservoir in the study area, in conjunction with image pore analysis and scanning electron microscopy, were conducted and are summarized in Table 2. The findings indicate that the reservoir space in each small layer of the Chang 8 reservoir is predominantly characterized by intergranular pores (Figures 6A, B), followed by dissolution pores. The combinations of pore types include intergranular pores + dissolved pores and dissolved pores + intergranular pores (Figures 6C, D). The average total surface porosity is 3.3%, generally reflecting low surface porosity. A comparison between the two layers reveals a higher face rate in the Chang 8_1 layer compared to the Chang 8_2 layer. Pore morphology is mainly triangular and quadrilateral, with pores commonly connected by narrow and short throats. The Chang 8 reservoir is characterized by nano-scale pore throats, resulting in a dense reservoir. Fluid seepage capacity is primarily controlled by relatively large pores. The mainstream throat radius falls within the range of 101–601nm, the average pore throat ratio is mainly between 102 and 199, and the average movable fluid saturation is 26.51%.

The throat, a narrow channel connecting two pores, serves as a pivotal factor influencing the reservoir's seepage capacity. The size and shape of the throat are intricately controlled by the contact relationship between rock particles, the type of cementation, and the inherent shape and size of the particles (Figures 6E, F). Throats are categorized into coarse, medium, thin, micro-thin, and microthroats based on their size. A throat with a radius >3 μm is identified as a coarse throat. When the throat radius ranges from 3 to 1 μm, it is considered a medium throat. Throats with a radius of 1 to 0.5 μm are termed fine throats. Fine throats with a radius of 0.5 to 0.2 μm. Microthroats have a throat radius less than 0.2 μm. These variations in throat characteristics significantly influence the seepage behavior of the reservoir.

According to the pressure-mercury curves illustrated in Figure 7, it is evident that the throat channels within the study area, within the study area, which serve as connections between pores, exhibit medium sorting characteristics. The skewness of these channels predominantly reflects a normal coarse skewness. This observation indicates an uneven distribution of throat sizes, with a greater prevalence of fine and microfine throat channels.

In addition, research on the results of previous studies has revealed that the throat radius of the Chang 8 reservoir in the Yanchi area of the Ji Plateau Oilfield is generally smaller. Consequently, the mean pressure is lower, while both discharge and driving pressure are higher, which indicates that the reservoir must overcome a larger capillary pressure in the seepage process (Chalmers et al., 2012; Loucks et al., 2009; Liu et al., 2019).

The throat characteristics of the Chang 8 reservoir in the study area are characterized by uneven size distribution, fineness and poor connectivity. These factors are critical contributors to the low permeability of the reservoir. Consequently, it is essential to quantitatively characterize the microscopic pore-throat features within this region to establish a comprehensive understanding of the geological conditions pertinent to the development of such tight reservoirs.

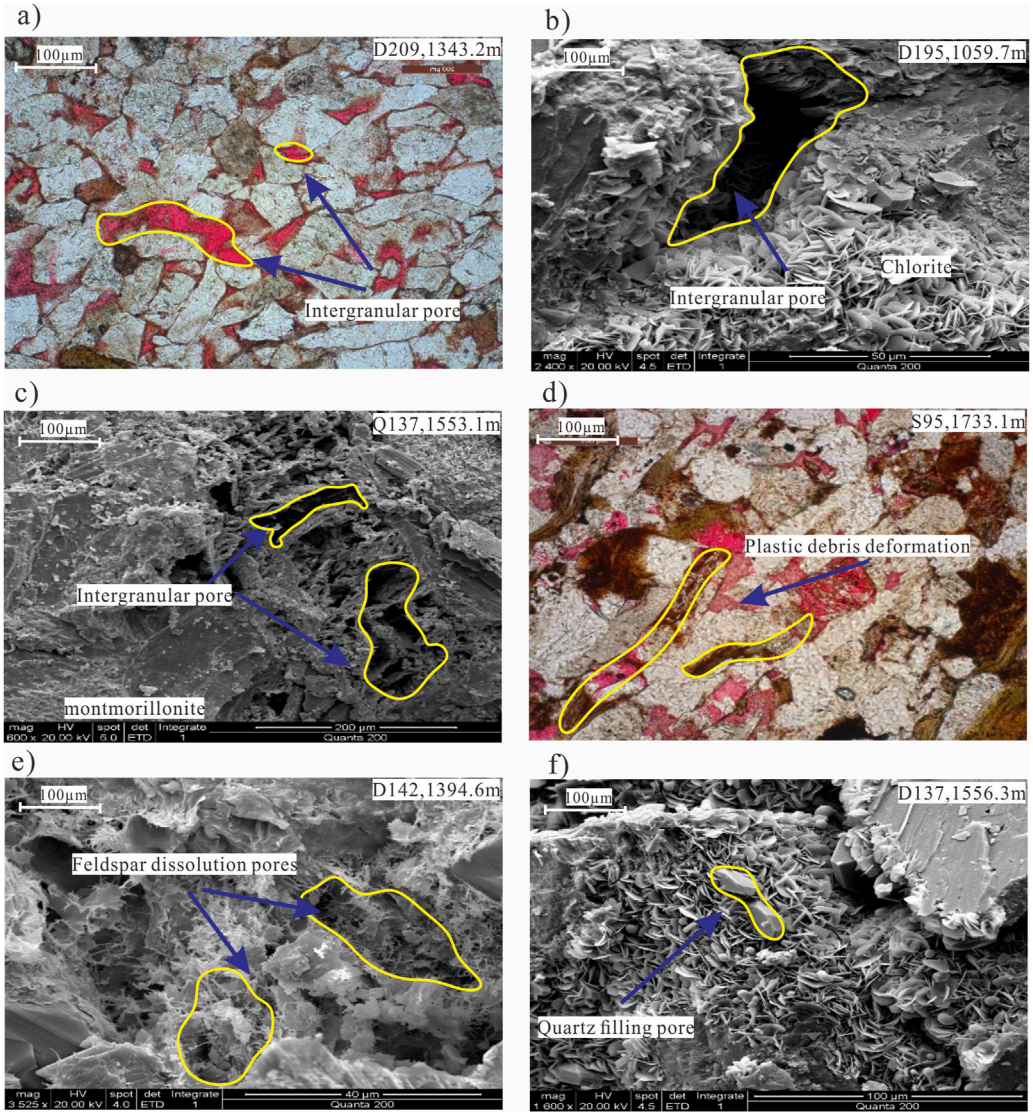

FIGURE 6
Microscopic pore structure characteristics of typical wells in Yanchi area. ((**a**). Intergranular pores, D209, 1343.2 m **(b)**. Intergranular pores, D195,1059.7m **(c)**. Intergranular dissolved pore, Q137,1553.12m **(d)**. Intragranular dissolved pores, S95,1733.07m **(e)**. Illite intracrystalline micropore, D142, 1394.55m **(f)**. Chlorite intergranular micropore, Q137, 1556.33 m).

TABLE 2 Chang 8 reservoir space type statistics (unit: %).

Horizon	Samples	Intergranular pore	Feldspar dissolution pores	Zeolite dissolved pore	Face rate
Chang 8_1	16	3.09	1.47	0.09	4.66
Chang 8_2	14	0.84	1.11	0	1.94
Average	—	1.96	1.29	0.04	3.30

The study of 20 samples in the Yanchi area has yielded characteristic parameters that reflect the intricate pore structure of the Chang 8 reservoir. By cross-referencing regional research data, the pore structure is effectively categorized into four distinct types, as illustrated in Figure 7. Based on the evolving characteristics of different mercury feed curves, the mercury feed process can be roughly divided into three stages: In the initial stage, when the capillary pressure reaches the discharge pressure, mercury is first introduced into the pore connected to the relatively large throat. At this time, the total capillary pressure curve and the pore capillary

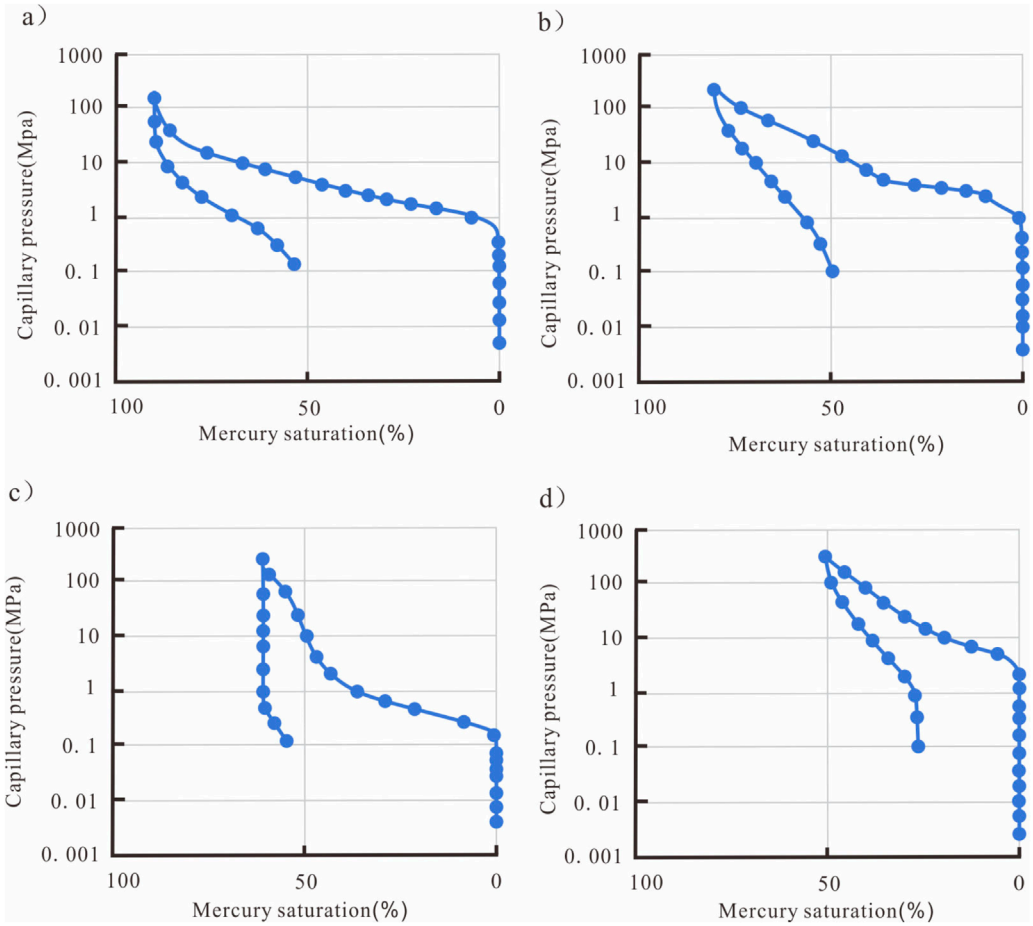

FIGURE 7
Type of capillary pressure curve of Chang 8 reservoir in Yanchi area. ((**a**) Type I mercury intrusion curve, D209,1343.3m **(b)** Type II mercury intrusion curve, D209,1344.2m **(c)** Type III mercury intrusion curve, Q130,1710.7m **(d)** Type IV mercury intrusion curve, Q137,1556.1 m).

pressure curve almost completely coincide, and the influence of the throat is not yet significant; in the second stage, with the gradual increase of the mercury feed pressure, the pore capillary pressure curve begins to show a rising trend. Despite the sharp increase in mercury feed pressure, the amount of mercury in the pores increased relatively slowly, which indicated that the throat began to be the main factor controlling the mercury feed process. At this point, the total capillary pressure curve gradually separates from the pore capillary pressure curve; in the third stage, when the connecting pores are completely filled with mercury, continued increases in inlet pressure allow the mercury to enter only the finer throats. At this point, the total capillary pressure curve is completely influenced by the throat capillary pressure curve.

By comparing the capillary pressure curves of samples with different permeabilities in the study area (see Figure 7), it can be found that in reservoirs with higher permeabilities (such as Figures 7B, D), the overlap section between the pore capillary pressure curves and the total capillary pressure curves is longer, which indicates that the pore capillary pressure has a greater influence on and control of the total capillary pressure, reflecting that pores account for a larger proportion of the effective reservoir space. In reservoirs with lower permeability (Figures 7A, C), the influence of throat capillary pressure on total capillary pressure is more significant, indicating that the throat occupies a larger proportion in the effective reservoir space.

Type I pore structure is low-discharge driving pressure-medium-small pore type belongs to the general low permeability reservoir. This type of capillary pressure curve is biased toward the lower left of the graph, well sorted, and coarsely skewed. Porosity is greater than 12%, permeability is greater than $0.3 \times 10^{-3}\mu m^2$, this type of reservoir has a low discharge pressure. Displacement pressure is less than 0.35-MPa, the maximum mercury saturation is greater than 85%. It is a high-quality reservoir in the Chang 8, but it is less abundant.

The type II pore structureis of the medium-discharge driving pressure-fine pore type belongs to the ultra-low permeability reservoir. The pressure curve of this type of capillary is relatively biased toward the upper right of the graph, with poor sorting and fine crookedness. The porosity is 8–12%, the permeability is $0.1–0.3 \times 10^{-3}\mu m^2$, the displacement pressure is 0.35~1MPa, and the maximum mercury saturation is 75–85%. This type of reservoir is the better reservoir in Chang 8 and is more abundant.

Type III pore structure is higher discharge pressure-microporous type belongs to ultra-low permeability reservoir.

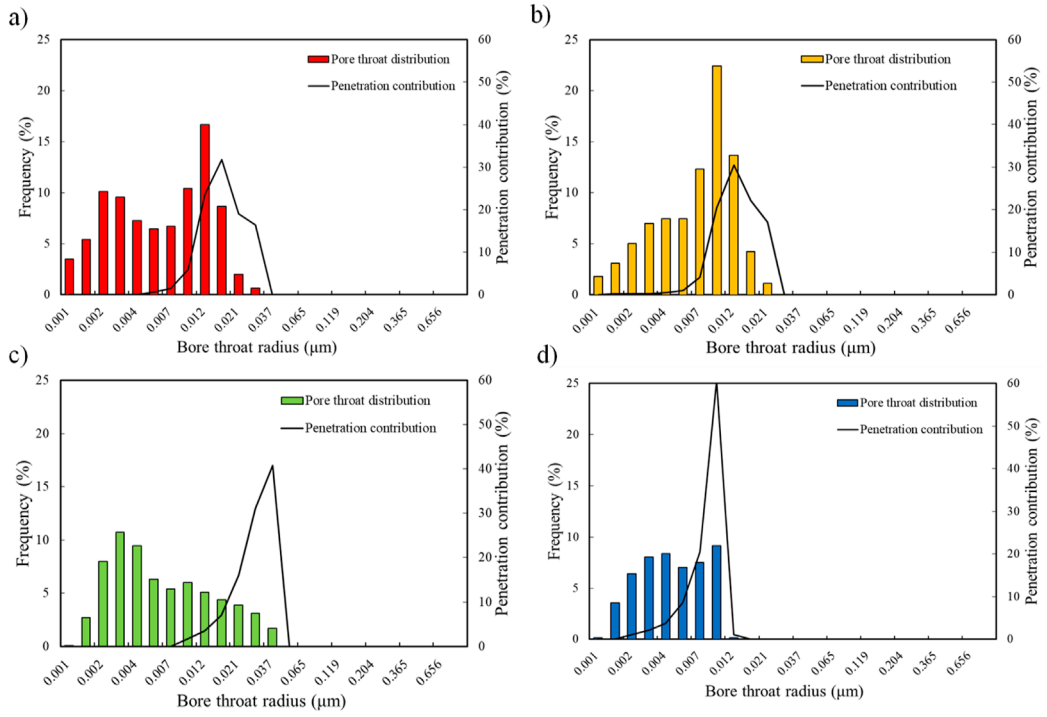

FIGURE 8
Distribution characteristics of pore throat radius in different types of reservoirs. ((**a**) D195, 1054.34m, Type I reservoir **(b)** D142, 1360.98m, Type II reservoir **(c)** Q54, 1454.19m, Type III reservoir **(d)** Q54, 1453.69m, Type IV reservoir).

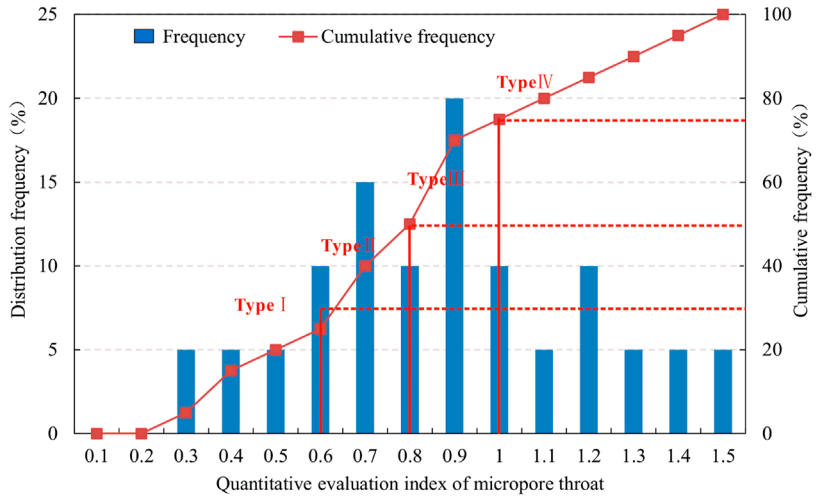

FIGURE 9
Comprehensive classification standard of pore throat quality.

The pressure curve of this type of capillary is relatively biased towards the upper right of the graph, with poor sorting and fine skewness. With porosity of 4–8%, permeability of 0.01–0.1 × 10^{-3}μm^2, displacement pressure of 1–1.5MPa, and maximum mercury saturation of 55–75%. This type of reservoir is the most abundant general reservoir in Chang 8.

The type IV pore structure is high discharge drive pressure-microporous type belongs to the tight reservoir, the porosity is less than 4%, the permeability is less than 0.01 × 10^{-3}μm^2, the displacement pressure is greater than 1.5MPa, and the maximum mercury saturation is less than 55%. This type is generally non-reservoir.

TABLE 3 Reservoir classification criteria of pore structure comprehensive evaluation index and pore throat quality factor.

Sorting parameter		Reservoir classification			
		I	II	III	IV
Physical characteristics	Porosity (%)	>12	8–12	4–8	<4
	Permeability (mD)	>0.3	0.1–0.3	0.01–0.1	<0.01
Pore Throat Index (*PTI*)		>1	0.8–1.0	0.6–0.8	<0.6
Comprehensive reservoir evaluation		Best	Good	General	Poor

In contrast to type III and type IV pore structures, type I and type II pore structures exhibit features such as lower displacement pressure and higher maximum mercury saturation. This observation suggests that type III pore structure is characterized by a more intricate pore structure, smaller pore throat radius, and inferior pore throat connectivity. The capillary pressure curve of type I and type II pore structures displays a plateau in the middle section, indicating relatively well-sorted pore throats. On the contrary, the capillary pressure curve of type III and type IV pore structures appears "oblique," signifying suboptimal pore-throat sorting.

The classification of pore structures was conducted on 20 mercury injection experimental samples obtained from coring wells (Supplementary Annex 2). The pore throat classification of the Chang 8 reservoir in the study area primarily falls into class II and class III, characterizing it as an ultra-low to low permeability reservoir. Data analysis indicates that the pore throat structure of the Chang 8_1 layer notably outperforms that of the Chang 8_2 layer. The displacement pressure within the target layer ranges from 0.04 to 8.94 MPa, with an average value of 1.20 Pa. The average maximum mercury saturation is 69.99%, and the average mercury removal efficiency is 21.17%. Generally, higher displacement pressure, lower maximum mercury saturation, and lower mercury removal efficiency signify poor reservoir seepage ability and a complex pore structure. The prevalent pore structures in the study area are type II and type III, categorizing it as a low porosity and ultra-low permeability reservoir. Among these, type II pore structure predominates, constituting 56.52%, followed by type III at 26.09%. Notably, the pore throat structure of the Chang 8_1 layer surpasses that of the Chang 8_2 layer.

Differences in the development of pore throats in different types of reservoirs lead to different physical properties of the reservoirs. Comparing the pore throat radius distribution of different types of reservoirs, it can be seen (Figure 8) that the reservoirs in the study area are dominated by nano-scale pore throats, and the reservoirs are relatively dense, and the differences in pore throat distribution of different types of reservoirs, the physical properties of Type I reservoirs are better, the distribution of pore throats is relatively wider, and the percentage of large pore throats is higher; with the decrease of physical properties, the distribution of pore throats of Type IV reservoirs is smaller as a whole, and the large pore throats are almost disappeared. The overall radius of the pore throat is less than 0.1μm, and the physical properties are the worst among the four types of reservoirs. For different reservoirs, the relatively large pore throats in the reservoir control the fluid seepage ability.

Due to the substantial volume of data obtained by conventional pore-throat characterization techniques and the difficulty of human analysis, we propose a method for the quantitative evaluation of microscopic pore throats in tight sandstones.This approach aims to analyze the pore types present in tight oil reservoirs by comprehensively assessing the pore throat parameters obtained through traditional characterization methods. Additionally, we introduce a quantitative evaluation index for microscopic pore throat quality that is both convenient and efficient, thereby enhancing the overall effectiveness of reservoir evaluations.

4.2 Quantitative evaluation of microscopic pore throat quality of tight sandstone reservoir

There are numerous parameters of the pore throat structure, mainly three types of parameters reflecting the pore throat size, sorting, connectivity and controlling the fluid movement characteristics. These different parameter characteristics can fully characterize the pore throat structure (Wang and Cheng, 2020). However, due to the complexity and diversity of the actual rock pore structure parameters, this study used the statistical method that quantitative assessment of the microscopic pore throat quality of tight sandstone reservoirs was conducted using pore structure parameters obtained from mercury injection experiments on 20 samples. Seven parameters, namely porosity (φ), median radius (R_{pt50}), displacement pressure (P_d), maximum pore throat radius (R_{max}), maximum mercury saturation (S_{max}), mercury removal efficiency (W_E), and permeability (K), were employed as characteristic variables for this evaluation. Notably, porosity (φ), median radius (R_{pt50}), displacement pressure (P_d), and maximum pore throat radius (R_{max}) were identified as influential factors on pore throat quality. To facilitate this assessment, a logging evaluation index, *PTI* (Pore Throat Index), was established, and a quantitative evaluation standard for the microscopic pore throat quality of tight sandstone reservoirs was developed (refer to Table). The reservoirs in the study area were categorized into four classes: I, II, III, and IV, based on *PTI* values (Figure 9). The comprehensive evaluation index of pore structure and the classification standard for the pore throat quality factor are detailed in Table 3. Specifically, a reservoir is classified as type I when $PTI > 1$, type II when $1 \leq PTI \leq 0.8$, type III when $0.8 < PTI < 0.6$, and type IV when $PTI < 0.6$. Higher *PTI* values indicate superior pore throat quality and contribute to an enhanced overall reservoir evaluation.

Type I reservoir, exemplified by Well D209 well and the 1342.5 m sample, exhibits characteristics of low displacement pressure, typically below 0.4 MPa, and a median pore throat radius exceeding 0.2μm, indicating a small to medium-sized pore structure. These reservoirs showcase permeability greater than 0.3×10^{-3}μm^2 and generally possess porosity exceeding 12%. The predominant pore type is intergranular pore-dissolved pore, and the Pore Throat Index (*PTI*) exceeds 1, designating it as a medium to high-quality reservoir within the Chang 8 formation. However, such reservoirs are relatively scarce in number.

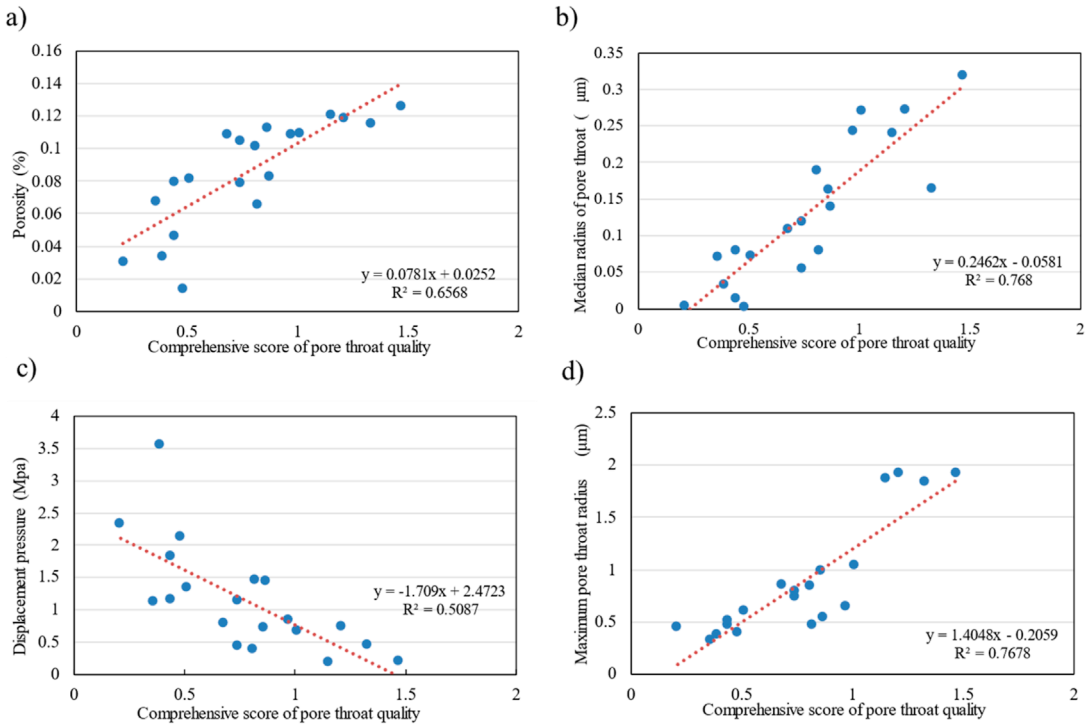

FIGURE 10
Relationship between pore throat quality comprehensive evaluation and pore structure parameters. ((**a**). Relationship between porosity and pore throat quality **(b)**. Relationship between median radius and pore throat quality **(c)**. Relationship between displacement pressure and pore throat quality **(d)**. Relationship between maximum pore throat radius and pore throat quality).

TABLE 4 Table of vector eigenvalues and variance contributions corresponding to the new parameters.

New parameter	Initial eigenvalue		
	Vector eigenvalue	Variance contribution (%)	Cumulative contribution (%)
1	4.850	69.285	69.285
2	1.008	14.405	83.690
3	0.486	6.938	90.628
4	0.291	4.157	94.785
5	0.183	2.610	97.395
6	0.101	1.437	98.832
7	0.082	1.168	100.000

Type II reservoir, exemplified by Well D209 and the 1344.2 m samples, features a displacement pressure ranging from 0.4 to 1 MPa and a median pore throat radius of 0.1–0.2μm, characterizing it as a fine-pore type. With permeability falling within the range of $0.1–0.3 \times 10^{-3}\mu m^2$, these reservoirs generally exhibit porosity levels of 8%–12%. The primary pore types include dissolved pores and intergranular pores, contributing to a Pore Throat Index (*PTI*) of 0.8–1. This reservoir type is prevalent in the Chang 8 formation and is considered a favorable reservoir.

Type III reservoir, exemplified by Well Q10 at a depth of 1710.7 m, is characterized by a displacement pressure ranging from 1 to 1.7 MPa and a median pore throat radius of 0.05–0.1 μm, classifying it as a fine-pore type. With permeability in the range of $0.01–0.1 \times 10^{-3}\mu m^2$, these reservoirs typically exhibit porosity levels of 4%–8%. The dominant pore type is dissolution pore, contributing to a Pore Throat Index (*PTI*) of 0.6–0.8. This reservoir type is common in the Chang 8 formation, representing the majority in terms of quantity.

TABLE 5 Principal component loadings matrix.

Pore structure parameters	Load weight value	
	Principal component 1	Principal component 2
Porosity (%)	0.952	−0.076
Median radius (μm)	0.919	−0.060
Displacement pressure (MPa)	−0.887	−0.085
Maximum pore throat radius (μm)	0.880	0.150
Maximum mercury saturation (%)	0.870	−0.094
Mercury withdrawal efficiency (%)	0.790	−0.436
Permeability ($\times 10^{-3}$μm2)	0.396	0.878

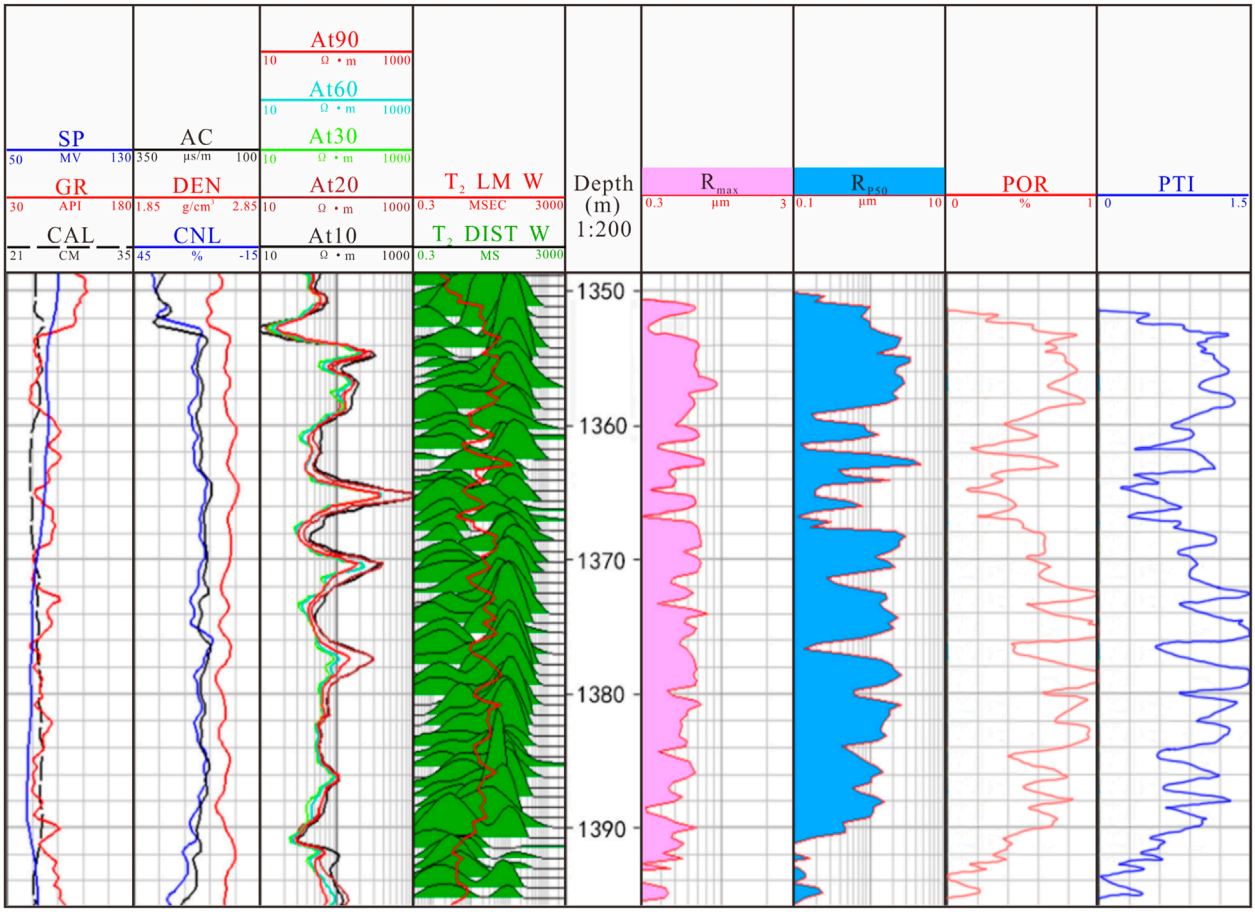

FIGURE 11
Comparison results of pore structure parameters of well D125 in the study area (R_{max}--Maximum pore throat radius; R_{pt50}--Median radius; *POR*--Porosity; *PTI*--Logging evaluation index of pore throat quality).

Type IV reservoirs, exemplified by Well Q137 at a depth of 1556.1m, are characterized by a displacement pressure exceeding 1.7 MPa and a median pore throat radius less than 0.05μm, indicating a microporous nature. With permeability below 0.01 × 10^{-3}μm^2, these reservoirs typically exhibit porosity levels less than 4%. The predominant pore type is micropore, contributing to a Pore Throat Index (*PTI*) of less than 0.6. This class represents a dense layer and is generally non-reservoir in nature.

4.3 Correlation between microscopic pore structure parameters and microscopic pore throat quality of tight sandstone reservoir

Upon conducting a quantitative evaluation and analysis of the microscopic pore throat quality in tight sandstone reservoirs, it has been deduced that porosity, pore throat median radius, displacement pressure, and maximum pore throat radius wield significant influence over microscopic quality (Dong et al., 2022; Lu et al., 2021). Consequently, the relationship curve between these four parameters and the comprehensive evaluation of the Pore Throat Quality Index (*PTI*) is established. Figure 10 illustrates that porosity, median radius of the pore throat, and maximum radius of the pore throat exhibit a positive correlation with the *PTI*, signifying that greater porosity, median radius, and maximum radius correspond to improved pore throat quality. In contrast, displacement pressure displays a negative correlation with *PTI*, indicating that lower displacement pressure is associated with better pore throat quality.

Porosity and permeability serve as determining factors for the physical properties of tight oil reservoirs. Enhanced reservoir physical properties are observed with increased porosity and permeability. Porosity plays a fundamental and crucial role in shaping reservoir pore structure characteristics and determining reservoir development potential by affecting reservoir space, pore connectivity, and pore size distribution.

The median radius of the pore throat can reflect the concentrated distribution degree and size of the pore throat, which is an important parameter to characterize the quality of pore structure and seepage capacity of the reservoir (Yin et al., 2018a). A larger value indicates improved rock pore structure, while a smaller value suggests the opposite.

Discharge pressure is closely related to the physical properties of the reservoir, and when the discharge pressure increases, the porosity decreases and the permeability decreases, and the mechanism of its influence on the permeability is different in different reservoir types. The fluid flow ability of reservoirs with different throat types under the action of discharge pressure varies greatly, with low discharge pressure reservoirs having better fluid flow ability, medium discharge pressure being the second best, and medium and high discharge pressure being worse. The study of the relationship between discharge pressure and reservoir pore structure is of great significance for reservoir evaluation and oil and gas development.

The maximum pore throat radius has a multifaceted impact on the pore structure of reservoirs. It can determine the flow resistance and transportation efficiency of fluids in the reservoir, affect the pore connectivity and inhomogeneity, enhance the permeability and fluid mobility of the reservoir, and play a decisive role in the production capacity and development of the reservoir (Meng et al., 2023; Yin et al., 2018b). The larger the maximum pore throat radius, the larger the pore structure, the stronger the connectivity, and the better the comprehensive evaluation of the reservoir (Yang et al., 2017).

5 Case analysis

Taking the reservoir physical properties and microscopic pore throat characteristic parameters of 13 sample data from the Chang 8 reservoir in the Yanchi area as the research focus, the data undergo standardization. The factor analysis method is then employed to reduce the data dimension, obtaining the initial eigenvalue of the correlation coefficient matrix (Table 4). The cumulative variance contribution rate of new parameter 1 and new parameter 2 among the seven newly constructed parameters is 83.69%, which indicates that the two constructed principal component variables can contain most of the geologic information in the original pore throat parameters, and the two newly constructed principal component variables can be used to replace the original seven pore structure parameter variables, which are called principal component 1 and principal component 2.

As shown in Table 5, the pore structure parameter loading weight values for main component 1 and main component 2, the numerical size represents the degree of contribution of different pore structure parameters to the main component, and the positive and negative symbols represent the positive and negative correlation with the main component, from which the formula for the calculation of a single main influence factor can be obtained. It is as follows:

$$F_1 = 0.432 * X_1 + 0.417 * X_2 - 0.403 * X_3 + 0.399 * X_4 + 0.395 * X_5 + 0.359 * X_6 + 0.18 * X_7$$

$$F_2 = -0.076 * X_1 - 0.06 * X_2 - 0.84 * X_3 + 0.149 * X_4 - 0.093 * X_5 - 0.434 * X_6 + 0.874 * X_7$$

The following inference formula for the pore-throat quality logging evaluation index PTI is obtained, and finally, the influencing factors are comprehensively analyzed to quantitatively characterize the influences of pore structure, maximum pore-throat radius, median radius, and discharge pressure on the microscopic pore-throat quality.

$$F = 69.285 * F_1 + 14.405 * F_2$$

Utilizing the pertinent data from Supplementary Annex 3 regarding reservoir physical properties and microscopic pore characteristic parameters, The *PTI* index is calculated using the above formula for the pore throat quality logging evaluation method, Subsequently, a comprehensive evaluation of the reservoir for these samples is conducted. The ultimate pore throat type aligns with the corresponding pore throat parameter characteristics of each type.

Figure 11 represents the interpretative diagram of the logging pore conclusion for well D209 in the Yanchi area. As depicted in the diagram, the pore structure parameters align well with the pore throat quality index. The larger the maximum pore throat radius, median radius, and porosity value, the more significant the T_2 spectrum reflects as large pores (Lu ZD. et al., 2022). Consequently, the higher the *PTI* index, the better the reservoir quality. Conversely, smaller values indicate small pores. Employing this method for evaluating the pore throat quality of 13 samples from 10 wells in the study area yielded results consistent with the quantitative evaluation outcomes of pore throat. The pore structure types reflected by the T_2 spectrum pore radius distribution and the microscopic pore throat quality logging evaluation method are in harmony with the pore structure parameters. The microscopic pore throat quality quantitative evaluation index effectively analyzes the pore types of tight oil reservoirs, exhibiting consistent results with those obtained through high-pressure mercury intrusion

nuclear magnetic resonance. Thus, the application of this method demonstrates satisfactory effectiveness.

Existing experimental analysis techniques for pore throat structure characterization have reached a high level of sophistication, characterized by high resolution and measurement accuracy. These methods are capable of quantitatively determining the pore structure parameters of tight reservoirs. Techniques such as cast thin section analysis and scanning electron microscopy can effectively analyze the material composition and structural characteristics of tight reservoirs; however, their effectiveness in characterizing microscopic pore throats is limited. On the other hand, mercury pressure and nuclear magnetic resonance techniques have the advantage that they can accurately and quantitatively characterize the microscopic pore-throat structure of tight reservoirs through experimental data. Nevertheless, these methods also have limitations, as each technique is restricted to a specific range of pore sizes that it can effectively test.

And the pore throat parameters derived from experiments such as piezomercury and NMR are large in data volume, which is difficult to analyze. The evaluation method of microscopic pore throat logging can comprehensively evaluate the pore structure parameters obtained from other characterization methods, quickly classify and evaluate the reservoirs, and the experimental analysis results are highly accurate, so it can be used for quantitative characterization of the microscopic pore throat of tight oil reservoirs. Therefore, it is essential to thoroughly understand the principles and applicability of different testing methods when investigating reservoir microstructures. By integrating various characterization techniques with considerations for differing rock types, we can enhance both the accuracy and scientific rigor in characterizing pore throat structures.

The pore structure of reservoir rocks directly determines the reservoir storage and seepage performance, and has a great influence on the oil production capacity, water-driven oil efficiency, and oil and gas recovery. At home and abroad, the pore microstructure, pore type, pore evolution and control factors, and storage performance parameters of tight sandstone reservoirs have become the focus of tight oil reservoir research (Webber et al., 2013; Chen et al., 2016; Zhan et al., 2022; Vargas-Florencia et al., 2007). Therefore, it is of great significance to carry out the quantitative characterization of the micropores and throats in tight oil reservoirs for the exploration and development of tight oil reservoirs.

6 Conclusion

(1) Through analysis, it has been determined that the parameters of porosity (φ), median radius (R_{pt50}), displacement pressure (P_d), and maximum pore throat radius (R_{max}) significantly influence pore throat quality. Consequently, the logging evaluation index PTI for pore throat quality has been established, along with the development of a quantitative evaluation standard for the microscopic pore throat quality of tight sandstone reservoirs. The reservoirs in the study area are categorized into four groups: I, II, III, and IV.

(2) When $PTI > 1$, it represents a Type I reservoir; when $1 \leq PTI \leq 0.8$, it corresponds to a Type II reservoir; when $0.8 < PTI < 0.6$, it signifies a Type III reservoir; when $PTI < 0.6$, it designates a Type IV reservoir. A higher *PTI* value indicates better pore throat quality and a more favorable overall evaluation of the reservoir.

(3) The quantitative characterization of the microporous structure of tight oil reservoirs using the microporous quality logging evaluation method has been applied with good results, and the construction of the quantitative evaluation standard of microporous quality of tight sandstone reservoirs can quickly analyze the pore structure of tight oil reservoirs and the type of reservoirs. The pore structure of the reservoir rock directly determines the storage and seepage performance of the reservoir, and has a great influence on the oil production capacity, water-driven oil efficiency, and oil and gas recovery rate. This method provides an important basis for the effective evaluation of reservoir development potential.

Data availability statement

The original contributions presented in the study are included in the article/Supplementary Material, further inquiries can be directed to the corresponding authors.

Author contributions

XZ: Conceptualization, Data curation, Formal Analysis, Funding acquisition, Investigation, Methodology, Project administration, Resources, Software, Supervision, Validation, Visualization, Writing–original draft, Writing–review and editing. XQ: Formal Analysis, Writing–original draft. ZW: Investigation, Writing–review and editing. XH: Data curation, Writing–review and editing. SL: Supervision, Writing–review and editing. CT: Formal Analysis, Supervision, Writing–review and editing. JP: Software, Writing–original draft. XL: Validation, Writing–original draft.

Funding

The author(s) declare that no financial support was received for the research, authorship, and/or publication of this article.

Conflict of interest

Author XZ was employed by China National Petroleum Corporation Oriental Geophysical Exploration Co. Ltd. Author XQ was employed by Ltd. Chuanqing Drilling and Exploration Engineering Co., Ltd. Changqing Downhole Technology Operation Company. Authors ZW, XH, and SL were employed by PetroChina Changqing Oilfield Company Plant No.7. Author JP was employed by China PetroChemical News.

The remaining authors declare that the research was conducted in the absence of any commercial or financial relationships that could be construed as a potential conflict of interest.

Generative AI statement

The author(s) declare that no Generative AI was used in the creation of this manuscript.

Publisher's note

All claims expressed in this article are solely those of the authors and do not necessarily represent those of their affiliated organizations, or those of the publisher, the editors and the reviewers. Any product that may be evaluated in this article, or claim that may be made by its manufacturer, is not guaranteed or endorsed by the publisher.

Supplementary material

The Supplementary Material for this article can be found online at: https://www.frontiersin.org/articles/10.3389/feart.2025.1510396/full#supplementary-material

References

Alessa, S., Sakhaee-Pour, A., Sadooni, F. N., and Al-Kuwari, H. A. (2021). Comprehensive pore size characterization of Midra shale. *J. Petroleum Sci. Eng.* 203, 108576. doi:10.1016/j.petrol.2021.108576

Bai, S. T., Cheng, D. J., Wan, J. B., Yang, L., Peng, H. L., Guo, X. K., et al. (2016). Quantitative characterization of nuclear magnetic resonance T_2 spectrum of sandstone rock. *Petroleum J.* 37 (3). doi:10.7623/syxb201603010

Chai, X. L., Tian, L., Meng, Y., Wang, J. Y., Huang, C., Wang, Z. C., et al. (2023). Microscopic pore structure characteristics and classification of tight reservoirs in Ordos Basin. *Nat. Gas. Geosci.*, 34, 1, 51–59. doi:10.11764/j.issn.1672-1926

Chalmers, G. R., Bustin, R. M., and Power, I. M. (2012). Characterization of gas shale pore systems by porosimetry, pycnometry, surface area, and field emission scanning electron microscopy/transmission electron microscopy image analyses: examples from the Barnett, Woodford, Haynesville, Marcellus, and Doig units. *AAPG Bull.* 96 (Issue 6), 1099–1119. doi:10.1306/10171111052

Chen, H. Q., Du, Y. J., and Wang, Y. (2016). Pore structure characteristics and its influence on science technology and engineering. *Sci. Technol. Eng.*, Volume 16, Issue 32, 28–35.

Chen, M., Dai, J., Liu, X., Kuang, Y., Qin, M. J., and Wang, Z. T. (2019). Contributions of pore-throat size distribution to reservoir quality and fluid distribution from NMR and MIP in tight sandy conglomerate reservoirs. *Arab. J. Geosci.* 12, 9. doi:10.1007/s12517-018-4153-7

Clarkson, C. R., Solano, N., Bustin, R. M., Bustin, A. M. M., Chalmers, G. R., He, L., et al. (2013). Pore structure characterization of North American shale gas reservoirs using USANS/SANS, gas adsorption, and mercury intrusion. *Fuel*, 103, Pages 606–616. doi:10.1016/j.fuel.2012.06.119

Deng, Y. R., Ren, Z. L., Ma, W. Q., Chen, X. P., and Yang, G. L. (2018). Nanka Owu. Tight sandstone reservoir characteristics and lower filling limit of Chang 8 member in Fuxian area, Ordos Basin. *Pet. Exp. Geol.*, Volume 40, Issue 2, 288–294. doi:10.11781/sysydz201802288

Dong, Y., Wang, R., Wang, S., Meng, W., Chen, L., and Tang, S. (2022). Study on synergistic oil displacement mechanism of CO_2-low interfacial tension viscoelastic fluid alternating flooding in ultra-low permeability sandstone reservoir. *Chem. Eng. Oil and Gas, Volume51* (6), 77–83. doi:10.3969/j.issn.1007-3426

Fan, Q., Ruan, Y., and Zhou, J. (2023). Current status and prospect of domestic natural gas purification plants under the target of carbon peaking and carbon neutralization. *Chem. Eng. Oil and Gas*, Volume 52, Issue 1, 25–31+39. doi:10.3969/j.issn.1007-3426

Hong, D., Cao, J., Wu, T., Dang, S., and Yao, S. (2020). Authigenic clay minerals and calcite dissolution influence reservoir quality in tight sandstones: insights from the central Junggar Basin, NW China. *Energy Geosci.*, Volume 1, 2, 8–19. doi:10.1016/j.engeos.2020.03.001

Huang, X., Gao, H., and Dou, L. B. (2020). Microscopic pore structure and water flooding characteristics of tight sandstone reservoirs. *J. China Univ. Petroleum Nat. Sci. Ed.*, Volume 44, Issue 1, 80–88. doi:10.3969/j.issn.1673-5005.2020.01.009

Jia, C. Z., Zou, C., Li, J. Z., Li, D. H., and Zheng, M. (2012). Assessment criteria, main types, basic characteristics and resource prospects of tight oil in China, Volume 33, Issue 3, Pages 343–350. doi:10.7623/syxb201203001

Jing, X., Gao, W., Li, H., and Sun, Y. (2023). Simulation and calculation of CO_2 absorption under high gravity environment by Aspen Plus software. *Chem. Eng. Oil and Gas*, Volume 52, Issue 1, 1–5. doi:10.3969/j.issn.1007-3426

Klaver, J., Hemes, S., Houben, M., Desbois, G., Radi, Z., and Urai, J. L. (2015). The connectivity of pore space in mudstones: insights from high-pressure Wood's metal injection, BIB-SEM imaging, and mercury intrusion porosimetry. *Geofluids* 15 (Issue 4), 577–591. doi:10.1111/gfl.12128

Kong, X., Wan, X., Guo, Z., Zeng, Z., and Xu, H., (2023). Adaptive evaluation and optimization of volumetric fracturing parameters in tight sandstone reservoirs. *Chem. Eng. Oil and Gas*, Volume 52, Issue 2, 81–86. doi:10.3969/j.issn.1007-3426

Lai, J., Wang, G. W., Chai, Y., Wu, D. C., Yao, Y. B., Zhang, Y. D., et al. (2014). Genetic mechanism analysis and quantitative evaluation of pore structure of tight sandstone reservoir-Taking Chang 8 reservoir group in Jiyuan area of Ordos Basin as an example. *Geol. J.*, Volume 88, Issue 11, 2119–2130. doi:10.19762/j.cnki.dizhixuebao

Lan, S., Song, D., Li, Zh., and Liu, Y. (2021). Experimental study on acoustic emission characteristics of fault slip process based on damage factor. Journal of Mining and Strata Control. *Engineering* 3 (3), 24–33. doi:10.13532/j.jmsce.cn10-1638/td

Li, C. Z., Liu, X. B., You, F. L., Wang, P., Feng, X. L., and Hu, Z. Z. (2022). Pore size distribution characterization by joint interpretation of micp and NMR: a case study of Chang 7 tight sandstone in the Ordos Basin. *Processes*, Volume 10, Issue 10, 1941–2037. doi:10.3390/pr10101941

Li, J. H., Wu, H. B., Li, Y., Tian, Y., and Zou, Y. (2020). Analysis of microscopic pore structure characteristics of tight reservoirs in the Hailar Basin. *J. China Univ. Min. Technol.*, Volume 49, Issue 4, 721–729 + 741. doi:10.13247/j.cnki.jcumt.001120

Liu, G. F., Wang, L. H., Sun, Z. B., and Wang, J. T. (2022). Research progress of pore throat structure in tight sandstone reservoirs. *Petroleum Sci. Bull.*, Volume 7, Issue 3, 406–419. doi:10.3969/j.issn.2096-1693

Liu, H. L., Yang, Y. Y., Wang, F. Q., Deng, X. Q., Liu, Y., Nan, J. X., et al. (2018). Microstructure characteristics and genesis analysis of tight sandstone reservoirs-Taking Chang 6 and Chang 8 members in Longdong area of Ordos Basin as an example. *Petroleum Explor. Dev.*, Volume 45, Issue 2, 223–234. doi:10.11698/PED

Liu, S., Zolfaghari, A., Sattarin, S., Dahaghi, A. K., and Negahban, S. (2019). Application of neural networks in multiphase flow through porous media: predicting capillary pressure and relative permeability curves. *J. Petroleum Sci. Eng.* 180, 445–455. doi:10.1016/j.petrol.2019.05.041

Liu, Y., Lin, C. Y., Lin, J. L., Lin, J. L., Huang, X., and Liu, B. B. (2023). Pore structure characteristics and genesis analysis of deep low permeability-tight sandstone in Xihu Sag, East China Sea Basin. *Nat. Gas. Geosci.*, Volume 10, Issue 10, 1–17. doi:10.11764/j.issn.1672-1926

Loucks, R. G., Reed, R. M., Ruppel, S. C., and Jarvie, D. M. (2009). Morphology, genesis, and distribution of nanometer-scale pores in siliceous mudstones of the Mississippian Barnett Shale. *J. Sediment. Res.* 79 (12), 848–861. doi:10.2110/jsr.2009.092

Lu, X. F., Dong, F. J., Bo, X. S., Cao, Y., and Huang, H. (2021). Quantitative characterization of the efect of micro pore structure on reservoir quality of tight sandstone reservoirs based on improved grey correlation theory. *Pract. Underst. Math.*, Volume 51, Issue 4, 99–108.

Lu, Z. D., Liu, C. J., Zang, Q. B., Wu, Y. P., Yang, X. Y., Yang, H., et al. (2022a). Application of high-pressure mercury injection and nuclear magnetic resonance technology in pore structure analysis of tight reservoirs: a case study of Heshui area in Ordos Basin. *Geol. Sci. Technol. Bull.*, Volume 41, Issue 3, 300–310. doi:10.19509/j.cnki.dzkq

Lu, Z. D., Liu, C. J., Zang, Q. B., Wu, Y. P., Yang, X. Y., Yang, H., et al. (2022b). Application of high-pressure mercury compression and nuclear magnetic resonance technology in analyzing pore structure of tight reservoirs: a case study of the Heshui area in the Ordos Basin. *Geol. Sci. Technol. Bull.* 41 (3), 300–310. doi:10.19509/j.cnki.dzkq.2021.0256

Lv, W. Y., Zeng, L. B., Zhou, S. B., Ji, Y. Y., Liang, F., Hui, C., et al. (2020). Microscopic fracture characteristics and controlling factors of tight sandstone reservoirs in southwestern Ordos Basin-A case study of Chang 8 reservoir in Honghe Oilfield. *Gas. Geosci.*, Volume 31, Issue 1, 37–46. doi : doi:10.11764/j.issn.1672-1926

Mahdaviara, M., Rostami, A., Keivanimehr, F., and Shahbazi, K. (2021). Accurate determination of permeability in carbonate reservoirs using Gaussian Process Regression. *J. Petroleum Sci. Eng.* 196, 107807. doi:10.1016/j.petrol.2020.107807

Meng, J., Zhang, L. Y., Li, R., Zhao, A. F., Zhu, B. W., Huang, P., et al. (2023). Microscopic pore structure characteristics and classification evaluation of tight sandstone reservoirs. *Special oil gas reservoirs*, Volume 30, Issue 4, 71–78. doi:10.3969/j.issn.1006-6535

Morozov, V., Jin, Z., Liang, X., Korolev, E., Liu, G., Kolchugin, A., et al. (2021). Comparison of source rocks from the lower silurian longmaxi formation in the yangzi platform and the upper devonian semiluksk formation in east European platform. *Energy Geosci.*, Volume 2, Issue 1, 63–72. doi:10.1016/j.engeos.2020.10.001

Nie, H., Li, D., Liu, Z., Zhang, G., Hu, W., Wang, R., et al. (2020). An overview of the geology and production of the Fuling shale gas field, Sichuan Basin, China. *Energy Geosci.*, Volume 2, Issue 1-2, 147–164. doi:10.1016/j.engeos.2020.06.005

Ouyang, S. Q., Lu, X. X., Zhang, Y. Y., Chen, l., Qu, Y. Q., and Sun, W. (2023). Impacts of the pore-throat structure on fluid mobility in tight sandstone: insight from an improved method based on rate-controlled porosimetry and nuclear magnetic resonance. *Energy and Fuels*, Volume 37, Issue 1, 273–290. doi:10.1021/acs.energyfuels.2c03285

Singh, A., Jha, N. K., Mandal, P. P., Esteban, L., and Desai, B. G. (2022). Pore throat characterization of bioturbated heterogeneous sandstone, Bhuj Formation, Kachchh India: an integrated analysis using NMR and HPMI studies. *J. Petroleum Sci. Eng.* 211, 110221. doi:10.1016/j.petrol.2022.110221

Vargas-Florencia, D., Petrov, O. V., and Furó, I. (2007). NMR cryoporometry with octamethylcyclotetrasiloxane as a probe liquid. Accessing large pores. *J. colloid interface Sci.* 305 (2), 280–285. doi:10.1016/j.jcis.2006.09.054

Wang, B., Lu, C., Huang, Z., and Hu, S. (2021a). Experimental study on damage evolution characteristics of rock under triaxial rheological disturbance. *J. Min. Strata Control Eng.* 3 (4), 28–43. doi:10.13532/j.jmsce.cn10-1638/td.20210525.001

Wang, D., Hao, B., and Liang, X. (2021b). Slurry diffusion of single fracture based on fluid-solid coupling. *J. Min. Strata Control Eng.* 3 (1), 25–38. doi:10.13532/j.jmsce.cn10-1638/td.20200429.001

Wang, F. Y., and Cheng, H. (2020). Pore throat structure and reservoir physical properties of tight sandstone in Yanchang Formation, Ordos Basin. *J. Jilin Univ. Earth Sci. Ed.*, Volume 50, Issue 3, 721–731. doi:10.13278/j.cnki.jjuese.20190141

Wang, L. G., Zhang, Y. Z., Zhang, N. Y., Zhao, C. Y., and Wu, W. S. (2020). Pore structure characterization and permeability estimation with a modified multimodal Thomeer pore size distribution function for carbonate reservoirs. *J. Petroleum Sci. Eng.* 193, 107426. doi:10.1016/j.petrol.2020.107426

Wang, L. S., Ye, Y. P., Qin, J. H., Gao, Y., Deng, Y., Li, Y. Y., et al. (2022). Microscopic pore-throat structure characterization and oil-bearing classification evaluation of continental shale oil reservoirs: a case study of Permian Lucaogou Formation in Jimsar Sag. *Junggar Basin Oil gas Geol.*, Volume 43, Issue 1, 149–160. doi:10.11743/ogg20220112

Wang, M. L., Liu, Y. T., Zhang, F. D., Li, J., Yang, S., and Shao, L. Y. (2015). Quantitative analysis of microscopic pore throat structure of tight oil reservoirs in Ordos Basin. *Mineralogical J.*, Volume 35, Issue 3, Pages 318–322. doi:10.16461/j.cnki.1000-4734

Wang, Y. S., Gao, Y., and Fang, Z. W. (2021c). Pore throat structure and classification of Paleogene tight reservoirs in Jiyang depression, Bohai Bay Basin, China. *Petroleum Explor. Dev.*, Volume 48, Issue 2, 308–322. doi:10.1016/s1876-3804(21)60025-3

Webber, J. B. W., Corbett, P., Semple, K. T., Ogbonnaya, U., Teel, W. S., Masiello, C. A., et al. (2013). An NMR study of porous rock and biochar containing organic material. *Microporous Mesoporous Mater.* 178, 94–98. doi:10.1016/j.micromeso.2013.04.004

Wu, T., Li, L., Li, W., Gai, Y., Chen, L., Pan, G., et al. (2021). A quantitative study on source rocks in the western Leong depression, northern South China Sea. *Energy Geosci.*, Volume 2, Issue 1, 73–82. doi:10.1016/j.engeos.2020.10.002

Yang, C. C., Zhang, Y. Y., and Liu, L. M. (2023). Quantitative evaluation method of Chang 8 tight oil reservoir quality in Huachi area. *Logging Technol.*, Volume 47, Issue 1, 79–85. doi:10.16489/j.issn.1004-1338.2023.01.013

Yang, Z. F., Zeng, J. H., and Han, F. (2017). Microscopic pore characteristics of tight sandstone reservoirs in the Chang 6-Chang 8 section of the southwestern Ordos Basin. *Gas. Geosci.*, Volume 28, Issue 6, 909–919. doi:10.11764/j.issn.1672-1926

Yin, S., Lv, D., and Ding, W. (2018a). New method for assessing microfracture stress sensitivity in tight sandstone reservoirs based on acoustic experiments. *Int. J. Geomechanics*, Volume 18, Issue 4, 1–10. doi:10.1061/(asce)gm.1943-5622.0001100

Yin, S. ., Xie, R., Wu, Z., Liu, J., and Ding, W. (2019). *In situ* stress heterogeneity in a highly developed strike-slip fault zone and its effect on the distribution of tight gases: a 3D finite element simulation study. *Mar. Petroleum Geol.*, Volume 99, Issue 1, 75–91. doi:10.1016/j.marpetgeo.2018.10.007

Yin, S., Zhao, J., Wu, Z., and Ding, W. (2018b). Strain energy density distribution of a tight gas sandstone reservoir in a low-amplitude tectonic zone and its effect on gas well productivity: a 3D FEM study. *J. Petroleum Sci. Eng.*, 70, Issue 1, 89–104. doi:10.1016/j.petrol.2018.06.057

Zhan, G. W., Gu, Z. Y., Pang, H. Q., and Cai, Z. H. (2022). Characteristics of pore structure in dense sandstone reservoirs and its influence on development. *J. Southwest Petroleum Univ. Nat. Sci. Ed.*, Volume 44, Issue 3, 70–84. doi:10.11885/.issn.1674-5086

Zhao, J. Y., Liu, Z. W., Xie, Q. C., and Zhou, J. P. (2014). The classification characteristics of microscopic pore throat structure of Chang 7 tight oil reservoir in Jiyuan Oilfield, Ordos Basin. *China Pet. Explor.*, Volume 19, Issue 5, 73–79. doi:10.3969/j.issn.1672-7703

Zhao, K., Jiang, P., Feng, Y., Sun, X., Cheng, L., and Zheng, J. (2021). Investigation of the characteristics of hydraulic fracture initiation by using maximum tangential stress criterion. *J. Min. Strata Control Eng.*, Volume 3, Issue 2, 23–35. doi:10.13532/j.jmsce.cn10-1638/td

Zhao, Z., Wu, K., Fan, Y., Yue, W., and Zeng, B. (2020). An optimization model for conductivity of hydraulic fracture networks in the Longmaxi shale, Sichuan basin, Southwest China. *Energy Geosci.*, Volume 1, Issue 1-2, 47–54. doi:10.1016/j.engeos.2020.05.001

Zhong, C., Du, P., Liu, Z., Zhu, S., and Qian, P. (2023). Interconnection between carbon neutrality and development of offshore oil and gas in China. *Chem. Eng. Oil and Gas*, Volume 52, Issue 4, 32–40+47. doi:10.3969/j.issn.1007-3426

Zhou, L. Y., Luo, S. C., Lin, W. C., Shan, S. S., Zhou, Y., and Ma, L. (2022). Tight sandstone reservoir classification method based on comprehensive evaluation index of pore structure. *Logging Technol.*, Volume 46, Issue 6, 707–713. doi:10.16489/j.issn.1004–1338

Zou, M., Xia, D. L., Pang, W., and Xu, T. (2019). Characterization method of microscopic pore throat structure of tight sandstone reservoir and its application-Taking Chang 8 layer in Honghe area of Ordos Basin as an example. *J. Xi 'an Petroleum Univ. Nat. Sci. Ed.* 34 (2), 46–53. doi:10.3969/j.issn.1673-064X

Zou, N., Zhu, R. K., Wu, S. T., Yang, Z., Tao, S. Z., Yuan, X. J., et al. (2012). Types, characteristics, genesis and prospects of conventional and unconventional hydrocarbon accumulations: taking tight oil and tight gas in China as an instance. *Editorial office of Acta Petrolei Sinica*, Volume 33, Issue 2, 173–187. doi:10.7623/syxb201202001

Zuo, J., Yu, M., Hu, S., Song, H., Wei, X., Shi, Y., et al. (2019). Experimental investigation on fracture mode of different thick rock strata. *J. Min. Strata Control Eng.*, Volume 1, Issue 1, 7–23. doi:10.13532/j.jmsce.cn10-1638/td